

ENVELOPE STRUCTURE OF THE MIRA VARIABLE U ORIONIS

P. F. BOWERS¹ AND K. J. JOHNSTON

E. O. Hulburt Center for Space Research, Naval Research Laboratory

Received 1987 September 10; accepted 1987 December 17

ABSTRACT

We have obtained simultaneous VLA measurements of the distributions of 1612 and 1665 MHz OH masers associated with U Orionis. Comparison of the distributions at these frequencies indicates that the shell radius at 1612 MHz is comparable to that at 1665 MHz, contrary to previous suggestions in the literature. At 1665 MHz we find an incomplete ring distribution near the stellar velocity of -39 km s^{-1} , in agreement with previous MERLIN measurements. By mapping the emission over a larger velocity range, we find the most extreme low-velocity components to be clustered near the center of the ring, indicating that radial expansion is the dominant kinematic component at the radius of the OH masers ($\sim 50 \text{ AU}$). We also find a velocity discontinuity in the angular distribution, in the sense that emission eastward of the star is on the near side and emission westward of the star is on the far side relative to the star-Earth distance. We propose a model for the maser region in which the OH is distributed in axisymmetric, biconical density concentrations embedded in an approximately spherical shell whose outflow velocity is about $8 \pm 1 \text{ km s}^{-1}$ in all directions. This model offers a qualitative basis for understanding not only the angular distribution but also the complex structure of the line profiles as a function of time.

Subject headings: masers — stars: individual (U Ori) — stars: long-period variables

I. INTRODUCTION

The characteristics of OH masers associated with the Mira variable U Orionis have proven to be unusual in several respects.

OH emission from the vibrational ground-state, rotational transitions at 1665 and 1667 MHz was discovered from this star in 1969 by Wilson *et al.* (1972) who found the emission at each frequency to be concentrated in two velocity ranges, typical of the profile structure of OH/IR stars. Pataki and Kolena (1974) subsequently reported a flaring of the 1612 MHz emission to a peak flux density of 22 Jy on 1974 May 22-23, much stronger than any previous measurement of the main-line emission and of the upper limit of $\sim 0.5 \text{ Jy}$ determined at 1612 MHz several years earlier by Wilson *et al.* Subsequent profiles showed two main components at 1612 MHz, but, interestingly, the average velocity (-44 km s^{-1}) was blue-shifted by 5 km s^{-1} relative to the average value of the preflare main-line emission (Cimerman 1979; Jewell *et al.* 1979).

Flaring or significant changes of the profile shape of OH emission is rarely seen in OH/IR stars. Monitoring of many OH/IR stars shows that the emission at 1612, 1665, and 1667 MHz usually varies nearly in phase with the optical/infrared light cycle, although the variation tends to be more regular at 1612 MHz (Harvey *et al.* 1974; Fillit, Proust, and Lépine 1977; Jewell *et al.* 1979; Herman and Habing 1985). Monitoring of the postflare emission from U Ori has shown that the 1612 MHz profile shape remained relatively stable and that the amplitude variations followed the optical light cycle, but unlike other OH/IR stars, the mean intensity has decreased at each successive cycle (Jewell *et al.* 1979; Jewell, Webber, and Snyder 1981; Herman and Habing 1985). Meanwhile, the structure of the main-line profiles has evolved with time, although the total velocity range in published profiles (-43 to -35 km s^{-1}) is

comparable to the preflare velocity range (see Jewell, Webber, and Snyder 1981). The integrated intensity of the main-line emission weakened after the flare but has since increased to near the preflare level. The intensity variations are not well correlated with the optical light cycle (Harvey *et al.* 1974; Jewell *et al.* 1979).

Results of interferometric measurements of this star also are unusual. Fix *et al.* (1980) found the angular extent of the emission region at 1665 MHz to be $\sim 0''.5$, significantly larger than the size of $0''.2$ determined at 1612 MHz by Reid *et al.* (1977) and by Bowers, Johnston, and Spencer (1983). This result was interpreted to contradict some pumping models which predict that the main-line emission should be closer to the star than the satellite emission at 1612 MHz. The significance of this result was unclear, however, because the measurements had been taken at different epochs of a star with unusual temporal behavior. For example, in 1975 Reid *et al.* (1977) found the 1612 MHz emission to be composed of components with sizes less than $0''.03$ and greater than $0''.3$, while no evidence for compact components was found in 1978 by Reid *et al.* (1979). Chapman and Cohen (1985) subsequently obtained simultaneous interferometric measurements at 1612 and 1665 MHz. They confirmed that the angular extent of the 1612 MHz region is smaller but did not determine the positions of the 1612 MHz masers relative to those at 1665 MHz.

To gain a better understanding of the structure and kinematics of the envelope of this peculiar star, we have used the Very Large Array to determine simultaneously the absolute positions of maser features at both these frequencies. The observations are discussed in § II. In § III we combine our absolute position measurements with accurate relative positions measured with the MERLIN array and discuss the results. The gross properties of the maser region are determined in § IV, and a model of the envelope is presented in § V. Implications of the model for our understanding of the pump mechanism and the mass-loss mechanism are discussed in § VI.

¹ Also at Sachs/Freeman Associates, Inc., Landover, MD 20785.

II. OBSERVATIONS

The 1612 MHz and 1665 MHz data were obtained during 1985 January 19 (epoch 1985.05), at which time U Orionis was near maximum visual light (phase = 0.1). The observations were made with the NRAO² Very Large Array in its spectral line mode and with the feeds receiving right circular polarization at each frequency. Thirteen antennas were selected in the A-configuration with baseline lengths which ranged from ~ 3 to 34 km. The bandwidth was divided into 128 frequency channels, and on-line Hanning smoothing was applied to the data. The bandwidth was 195 kHz, resulting in a channel-to-channel frequency separation and resolution of 1.53 kHz and a velocity resolution of ~ 0.28 km s⁻¹ at 18 cm.

U Ori was observed for 30 minutes at each frequency, giving a rms noise fluctuation of 60 mJy per beam per channel. Phase calibrations were obtained with the continuum point source 0552 + 398. The flux density scale was established from observations of 3C 286 whose adopted flux density was 13.83 Jy at 1612 MHz and 13.61 Jy at 1666 MHz. The flux density of the phase calibrator was determined to be about 1.86 ± 0.03 Jy at these frequencies. Maps of the calibrated data were then made for each spectral channel, with natural weighting in the uv -plane. The maps were cleaned with the standard algorithm of Högbom (1974) and restored with a Gaussian beam shape with a full width half-power beamwidth of 1''.1.

III. RESULTS

The emission profiles at 1612 and 1665 MHz are shown in Figure 1. All 1612 MHz profiles published since 1974 have shown a double-peaked structure with components at about -47 and -42 km s⁻¹ (see, Jewell, Webber, and Snyder 1981;

Chapman and Cohen 1985). Our profile shows weak emission between -41.7 and -40.9 km s⁻¹ and no emission stronger than 0.3 Jy at -47 km s⁻¹, suggesting that the emission at this frequency is continuing to weaken with time.

The emission profile at 1665 MHz is complex, showing major features at about -46.5 , -41.5 , -39 , -37 , and -35 km s⁻¹. The feature at -46.5 km s⁻¹ is new. Previously published profiles only show emission between about -43 and -35 km s⁻¹ (Wilson *et al.* 1972; Fix 1979; Cimerman 1979; Jewell *et al.* 1979; Fix *et al.* 1980; Jewell, Webber, and Snyder 1981; Clausen and Fix 1982; Chapman and Cohen 1985). The features at -41.5 and -35 km s⁻¹ appear to correspond to the outer peak features measured from the preflare profiles of Wilson *et al.*, and which are indicated by the arrows. The -35 km s⁻¹ emission disappeared after the flare but reappeared several years later at a much weaker level (Jewell, Webber, and Snyder 1981). Emission at intermediate velocities (-39 km s⁻¹) was present in the preflare profiles, but its intensity ratio relative to the outer peaks increased from 0.2 to ~ 1 after the flare. Figure 1 shows that this emission is still comparable to or greater than the emission at the velocities of the preflare peak features.

Previous interferometric measurements have shown the structure at 1665 MHz to be complex. Fix *et al.* (1980) used VLBI techniques to map the emission between -43 and -39 km s⁻¹ and found features spread over 0''.5 with a velocity gradient from the southeast to the northwest. Chapman and Cohen (1985) used the MERLIN array to map the emission between -43.4 and -36.0 km s⁻¹ with a spatial resolution of $\sim 0''.3$. They found an incomplete ring structure of diameter 0''.45 and noted that there was some evidence for this structure in the earlier VLBI measurements of Fix *et al.* They also confirmed the existence of a velocity gradient around the ring, from -39 km s⁻¹ in the northwest to -43 km s⁻¹ in the southeast.

² The National Radio Astronomy Observatory is operated by Associated Universities, Inc., under contract to the National Science Foundation.

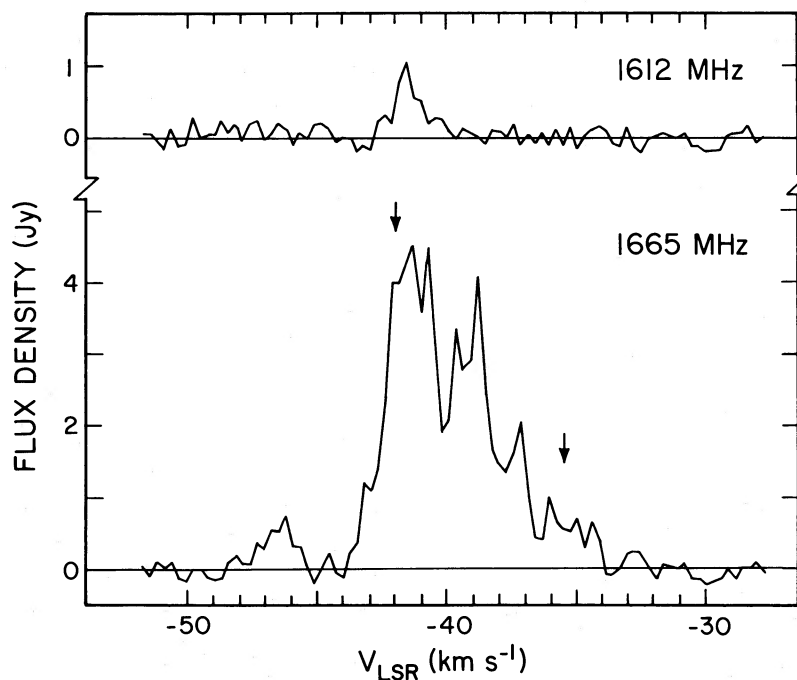


FIG. 1.—VLA spectral-line profiles of the right circularly polarized component of OH maser emission from U Ori at epoch 1985.05. Velocity resolution is 0.284 km s⁻¹ at the rest frequency of 1612.231 MHz and 0.275 km s⁻¹ at 1665.402 MHz.

TABLE 1
ABSOLUTE POSITIONS^a OF OH(1665 MHz)
MASERS FOR U ORIONIS

V_{LSR} (km s^{-1})	$\Delta\alpha$	$\Delta\delta$	Flux Density
-47.3	-0 ^h 10	-0 ^m 20	0.4
-47.0	-0.10	-0.20	0.3
-46.8	-0.10	-0.15	0.6
-46.5	-0.15	-0.10	0.5
-46.2	-0.10	-0.10	0.8
-45.9	-0.10	-0.10	0.3
-45.6	-0.20	-0.10	0.3
-43.4	-0.10	-0.25	0.5
-43.2	-0.05	-0.25	1.2
-42.9	0.00	-0.25	1.1
-42.6	0.00	-0.20	1.4
-42.4	-0.05	-0.15	2.4
-42.1	-0.10	-0.10	4.0
-41.8	-0.05	-0.10	4.0
-41.5	-0.05	-0.05	4.2
-41.2	-0.05	-0.05	4.5
-41.0	-0.05	-0.05	3.6
-40.7	-0.05	0.00	4.4
-40.4	0.00	0.00	3.2
-40.2	0.00	0.00	1.9
-39.9	-0.10	0.05	2.1
-39.6	-0.15	0.05	3.4
-39.3	-0.20	0.05	2.8
-39.0	-0.25	-0.10	2.9
-38.8	-0.25	-0.10	4.1
-38.5	-0.30	-0.10	2.9
-38.2	-0.25	-0.05	1.7
-38.0	-0.20	-0.15	1.5
-37.7	-0.10	-0.30	1.4
-37.4	-0.05	-0.30	1.6
-37.1	-0.10	-0.30	2.0
-36.8	-0.10	-0.25	1.1
-36.6	-0.10	-0.25	0.5
-36.3	-0.15	-0.25	0.4
-36.0	-0.10	-0.30	1.0
-35.8	-0.10	-0.20	0.6
-35.5	-0.10	-0.20	0.6
-35.2	-0.20	-0.20	0.5
-34.9	-0.20	-0.20	0.7
-34.6	-0.20	-0.30	0.3
-34.4	-0.20	-0.25	0.7
-34.1	-0.30	-0.20	0.4

^a Relative to $\alpha = 05^{\text{h}}52^{\text{m}}50^{\text{s}}.92$, $\delta = +20^{\circ}10'06''.0$; epoch 1950.

The absolute positions of 1665 MHz components as determined with the VLA are listed in Table 1 and plotted in Figure 2. All features were unresolved, and the positional error is estimated to be about $\pm 0''.05$. The empty circles represent components over the same velocity range mapped by Chapman and Cohen. Our positional errors are about twice as large as theirs, but comparison of the maps shows reasonably good agreement for $\Delta\alpha > -0''.2$. A partial ringlike structure and a velocity gradient are apparent as one follows the emission components from -39 km s^{-1} in the north to -43 km s^{-1} in the southeast. As noted by Chapman and Cohen, the velocity gradient is not continuous because of the -37 km s^{-1} emission detected toward the southern portion of the ring.

Largest discrepancies between the VLA and MERLIN maps occur at $V \approx -39$ to -38 km s^{-1} ($\Delta\alpha < -0''.2$) and $V \approx -37$ to -36 km s^{-1} . These discrepancies may be the result of the appearance of new maser components or of spatial blending caused by the poorer ($1''$) resolution of the VLA. At $V \approx -39 \text{ km s}^{-1}$, the VLA components fall midway between spatially

separated maser components in the MERLIN map at the same velocity, suggestive of spatial blending. At $V \approx -36 \text{ km s}^{-1}$, the VLA components are $\sim 0''.1$ northwest of the MERLIN components. This might suggest the appearance of new maser components at $V \approx -36 \text{ km s}^{-1}$, but their exact location is uncertain because of possible spatial blending effects. At other velocities, the agreement of our map with those of Fix *et al.* (1980) and Chapman and Cohen (1985) indicates that the velocity structure seen in the angular distribution has not changed with time.

The filled circles in Figure 2 represent velocity components whose positions have not previously been determined. The low-velocity features (-47.3 to -45.6 km s^{-1}) are clustered near the center of the overall distribution, while the high-velocity features (-35.8 to -34.1 km s^{-1}) tend to be located in the southwest portion of the distribution. Indeed, Figure 2 shows that features with $V > -39 \text{ km s}^{-1}$ are preferentially located south and west of the center, while features with $-43 < V < -39 \text{ km s}^{-1}$ are located north and east. Thus the east-west velocity discontinuity indicated by Chapman and Cohen for the southern portion of the shell appears to extend over the entire shell.

To delineate more clearly the emission distribution at 1665 MHz, we combine in Figure 3 the more accurate relative positions of Chapman and Cohen (*empty circles*) with the VLA absolute positions for the extreme low and high velocity emission not detected by them (*filled circles*). To align the two sets of observations, we have assumed that the strongest feature which they detected (at -39.5 km s^{-1}) is at the same position as the feature which we detected at -39.6 km s^{-1} ($\Delta\alpha = -0''.15$, $\Delta\delta = +0''.05$). The diagonal line at a position angle of -30° indicates the east-west velocity discontinuity for features at $V < -39 \text{ km s}^{-1}$ and $V > -39 \text{ km s}^{-1}$. The partial ringlike structure at intermediate velocities (*empty circles*) is readily evident.

We also have plotted in Figure 3 the available VLA and MERLIN 1612 MHz data. The solid triangles give the absolute positions determined with the VLA for the 1612 MHz emission (Table 2). Within the uncertainties, the positions of the 1612 MHz components agree with those at 1665 MHz. The -47 km s^{-1} feature at 1612 MHz was too weak to be detected by us, but Chapman and Cohen determined the positions of its components relative to the -41.5 km s^{-1} feature at 1612 MHz. We have plotted their data on Figure 3 by assuming that their position for the -41.5 km s^{-1} feature is coincident with our position for the -41.4 km s^{-1} feature.

The offset between the positions of -47 km s^{-1} emission at 1612 and 1665 MHz is slightly larger than expected from the errors in the relative positions internal to the two sets of data. This could be caused by polarization effects, proper motion,

TABLE 2
ABSOLUTE POSITIONS^a OF OH(1612 MHz) MASERS
FOR U ORIONIS

V_{LSR} (km s^{-1})	$\Delta\alpha$	$\Delta\delta$	Flux Density (Jy)
-41.7	0 ^h 00	0 ^m 00	0.8
-41.4	0.00	0.00	1.0
-41.2	0.00	0.00	0.6
-40.9	0.00	-0.05	0.5

^a Relative to $\alpha = 05^{\text{h}}52^{\text{m}}50^{\text{s}}.92$, $\delta = +20^{\circ}10'06''.0$; epoch 1950.

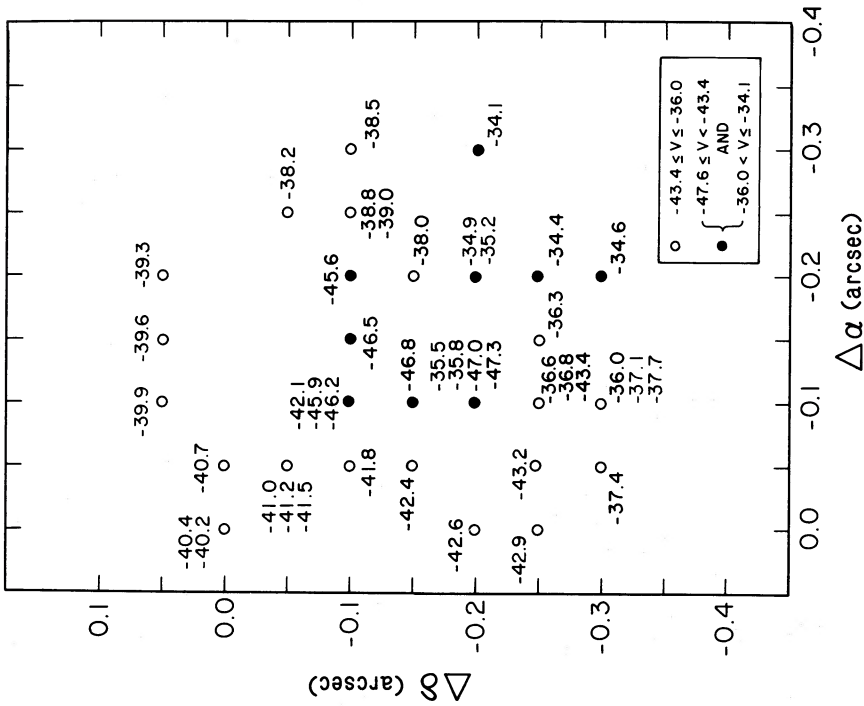


FIG. 2

FIG. 2.—Absolute positions of the 1665 MHz maser components of U Ori during epoch 1985.05. Open circles represent components over the same velocity range mapped by Chapman and Cohen (1985). Filled circles represent components whose positions have not been previously determined. Positional errors are approximately ± 0.05 , and the map origin is $\alpha(1950) = 05^h52^m50^s.920$ and $\delta(1950) = +20^\circ10'06''.00$.

FIG. 3.—Combined VLA and MERLIN data sets for the angular distributions of 1612 MHz and 1665 MHz emission components in the circumstellar envelope of U Ori. The map origin is identical to that of Fig. 2. Alignment of the VLA and MERLIN data sets at 1665 MHz is based on the assumed positional coincidence of components at -39.5 km s^{-1} (MERLIN) and -39.6 km s^{-1} (VLA). At 1612 MHz the alignment is based on assumed positional coincidence at -41.5 km s^{-1} (MERLIN) and -41.4 km s^{-1} (VLA). The diagonal line indicates the sense of the east-west velocity discontinuity. The VLA data were obtained at epoch 1985.05 and have relative positional errors of about ± 0.05 . The MERLIN data were obtained at epochs of ~ 1982.95 (1612 MHz) and 1983.12 (1665 MHz) and have positional errors of about ± 0.025 . The "X" denotes the position of the star inferred from the maser components (§ IVc).

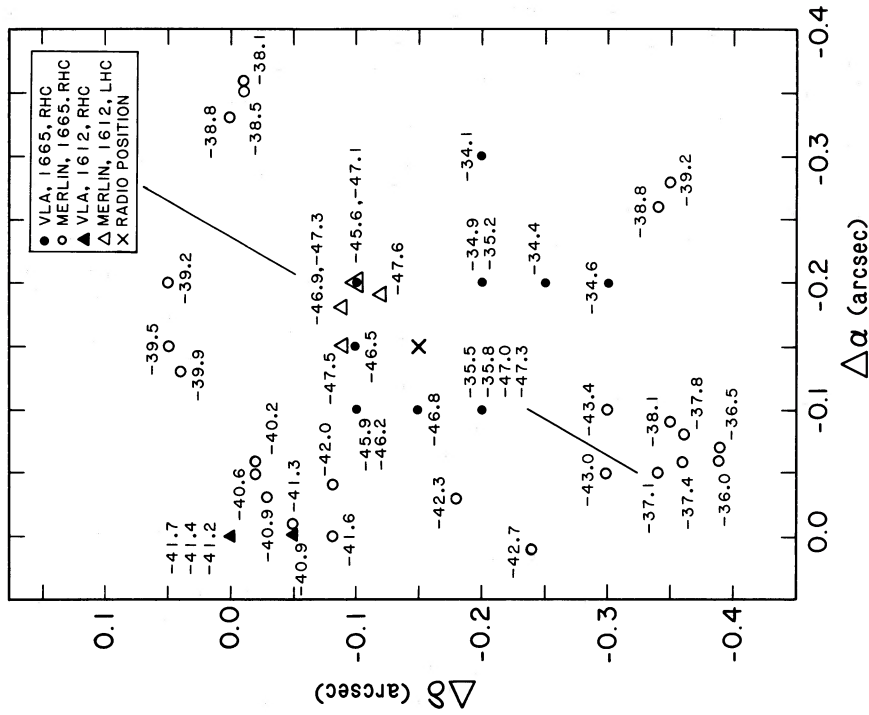


FIG. 3

velocity fluctuations, or marginally different spatial distributions at the two frequencies. Nonetheless, it is evident from Figure 3 that the 1612 MHz and 1665 MHz features are distributed over essentially the same velocity field and that the radius of the 1612 MHz emission region is comparable to, if not slightly larger than, that at 1665 MHz. At most position angles there simply is insufficient gain to produce emission at 1612 MHz. *Previous suggestions that the 1612 MHz shell is smaller than that at 1665 MHz were based only on the smaller angular extent at 1612 MHz* (Fix *et al.* 1980; Chapman and Cohen 1985).

IV. GROSS PROPERTIES OF THE ENVELOPE

In the standard case of the expanding spherical shell model, the gas radially expands from the star at a constant velocity V_e and a doubly peaked emission profile is produced with peaks at velocities of $V_0 \pm V_e$, where V_0 is the systemic radial velocity of the star (e.g., Kwok 1976; Reid *et al.* 1977). The peaks are positionally coincident and indicate the stellar position; at intermediate velocities ring-structures are centered about the stellar position with the maximum ring radius occurring at the stellar velocity.

The clustering in Figure 3 of the extreme low-velocity (-47 km s^{-1}) components near the center of the incomplete ringlike structure seen at intermediate velocities is a strong indication that radial expansion is an important kinematic component in the OH maser region. However, complexities in the profile structure and in the angular distribution at 1665 MHz also indicate significant deviations from the standard expanding shell model. These complexities have made it difficult to determine even the most fundamental parameters of the envelope (i.e., V_0 and V_e). In this section we discuss the extent to which available data provide information about such quantities.

a) Systemic Radial Velocity

The issue of the correct values of V_0 and V_e has been confused by changes in the structure of the OH emission profiles. However, there are now observations at a number of epochs for various transitions of OH, H_2O , and SiO, which provide a better determination of these quantities. We summarize in Figure 4 the largest velocity range over which emission from a given transition has been observed, with the circles denoting the preflare peaks of the main-line emission and the dashed lines indicating the midpoint of each velocity range. References for the low or high velocity extremes are as follows: OH (1612), Jewell *et al.* (1979) and Cimerman (1979); OH (1665), this paper; OH (1667), Wilson *et al.* (1972) and Fix (1979); SiO ($v=0$), Nyman and Olofsson (1985); H_2O Nyman and Olofsson (1986) and Lada *et al.* (1981); SiO ($v=1, J=1-0$), Snyder *et al.* (1986); SiO ($v=1, J=2-1$), Nyman and Olofsson (1986).

We also indicate the probable location of the emission at each transition. The mean radius of the OH distribution is $\sim 0''.21$ (Fig. 3 and § IVd), corresponding to a linear radius of 54 AU at a distance of $\sim 250 \text{ pc}$ (Bowers and Hagen 1984). The location of the ($v=1$) SiO masers has not been determined for U Ori but is likely to be close to the star based on interferometric measurements of similar stars (Lane 1982). Using VLBI techniques, Lada *et al.* (1981) measured the overall size of the H_2O maser region to be $0''.3$, corresponding to a radius of $\sim 40 \text{ AU}$. This value is comparable to values of 25–50 AU found for similar stars by Johnston, Spencer, and Bowers (1985) and Lane *et al.* (1987), suggesting that the H_2O radius is comparable to or slightly smaller than the OH radius. The location of

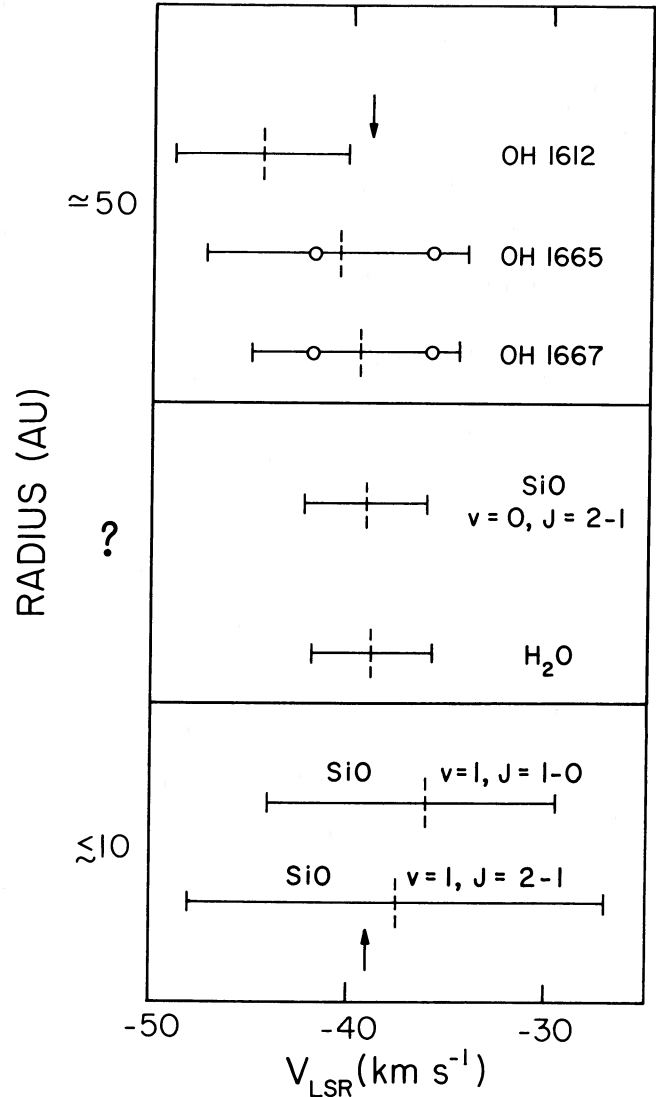


FIG. 4.—Largest observed velocity ranges of the indicated transitions of OH, H_2O and SiO and estimated locations of this emission in the envelope of U Ori. Circles indicate the velocities of the preflare peaks (Wilson *et al.* 1972), and dashed lines indicate the midpoints of the velocity ranges. Arrows indicate the adopted stellar radial velocity.

the ($v=0$) SiO emission is unknown but is probably comparable to that of the OH and H_2O based on its similar velocity range. The distribution of this emission is discussed further in § V.

The preflare, main-line OH emission had a doubly peaked structure with the outermost peaks (*circles*) at -42.0 and -35.5 km s^{-1} , giving $V_0 = -38.8 \text{ km s}^{-1}$ and " V_e " = 3.2 km s^{-1} . Figure 4 clearly shows that OH emission has since been detected over as much larger velocity range, and it is not symmetrically distributed relative to the original value of V_0 . Nonetheless, data for the other molecules support a value of $V_0 \approx -39 \pm 1 \text{ km s}^{-1}$, indicated by the arrow in Figure 4. This value agrees with the value of $-39.2 \pm 0.8 \text{ km s}^{-1}$ determined for the ($v=0$) SiO transition by Nyman and Olofsson (1985) and with the mean value of -38.8 km s^{-1} found from all published observations of the H_2O masers (Fig. 4). It also is close to the value of -38 to -37 km s^{-1} determined from the

time-averaged SiO maser profiles for the $v = 1, J = 1-0$ transition (Snyder *et al.* 1986) and the $v = 1, J = 2-1$ transition (Nyman and Olofsson 1986). The latter authors indicate that the value found from SiO masers tends to be redshifted by $\sim 1 \text{ km s}^{-1}$ on the average. Finally, a value of about -39 km s^{-1} is indicated by the ringlike distribution of the intermediate velocity features (Chapman and Cohen 1985) and by the east-west velocity discontinuity apparent in Figure 3. In the remainder of this paper we adopt $V_0 = -39 \text{ km s}^{-1}$ as the systemic radial velocity of U Orionis.

b) Expansion Velocity

The issue of the correct value for the expansion velocity is more difficult to resolve. Relative to $V_0 = -39 \text{ km s}^{-1}$, the -47 km s^{-1} component at 1665 MHz (Fig. 1) indicates an outflow velocity of at least 8 km s^{-1} , and Figure 4 shows that an apparent outflow velocity as large as 10 km s^{-1} has been detected at 1612 MHz—much larger than the preflare estimate. An outflow velocity of $\sim 10 \text{ km s}^{-1}$ also has been suggested by Wallerstein (1985) based on optical radial velocity data, but this gas is probably located much closer to the star in the complex velocity field of the ($v = 1$) SiO masers (see Fig. 4).

The ($v = 0$) SiO emission previously has been thought to be a good indicator of V_e (Reid and Dickinson 1976; Morris *et al.* 1979), and the total velocity range of this emission typically agrees well with the total velocity range at 1612 MHz (Bowers, Johnston, and Spencer 1983). However, Nyman and Olofsson (1985) find the profile shape of the ($v = 0$) $J = 2-1$ transition to be triangular rather than parabolic with a half-width of only 3.1 km s^{-1} , in agreement with the preflare OH value. They suggest possible maser action which could make the determination of V_e unreliable. On the other hand, Bujarrabal *et al.* (1986) argue that such profiles are thermal in nature. We propose a resolution to this problem in § V and conclude that the expansion velocity is approximately $8 \pm 1 \text{ km s}^{-1}$.

c) Stellar Position

Complexities in the OH data make it difficult to obtain a highly accurate stellar position for this star. For other stars there is evidence that the stellar position is best determined by the positions of the extreme low and high velocity emission features rather than the peak features, because of velocity fluctuations which can perturb the positions of the peak features (Bowers, Johnston, and Spencer 1983; Diamond *et al.* 1985). For U Ori, the most extreme velocity component yet detected relative to V_0 is at -49 km s^{-1} (Fig. 4); its position has not been determined. The distribution of components at $-47 \pm 0.5 \text{ km s}^{-1}$ in Figure 3 is scattered about a mean position of $\Delta\alpha = -0''.15$, $\Delta\delta = -0''.15$, consistent with the possibility that yet lower velocity gas would be located near the center of this distribution. This position also agrees with the average position of the most extreme low velocity features mapped at 1612 and 1665 MHz and is very near the geometric center of the overall distribution of features in Figure 3. We therefore adopt this as the stellar position, indicated by the "X." The resulting coordinates are $\alpha(1950) = 05^{\text{h}}52^{\text{m}}50^{\text{s}}.909$, $\delta(1950) = +20^{\circ}10'05''.85$ at the Besselian epoch of 1985.05. We attribute an error of $\pm 0''.05$ to this position based on the accuracy of our measurements. Additional errors may be introduced from the alignment of the VLA and MERLIN data sets (§ III), or from undetermined complexities in the shell structure.

d) Radius-Velocity Relationship

A plot of the 1665 MHz angular radius as a function of velocity is shown in Figure 5, where the angular radius is measured relative to the adopted stellar position. The shape of the curve is obviously quite sensitive to the adopted stellar position. We find that for assumed stellar positions greater than $0''.3$ from our adopted position the scatter in the data points

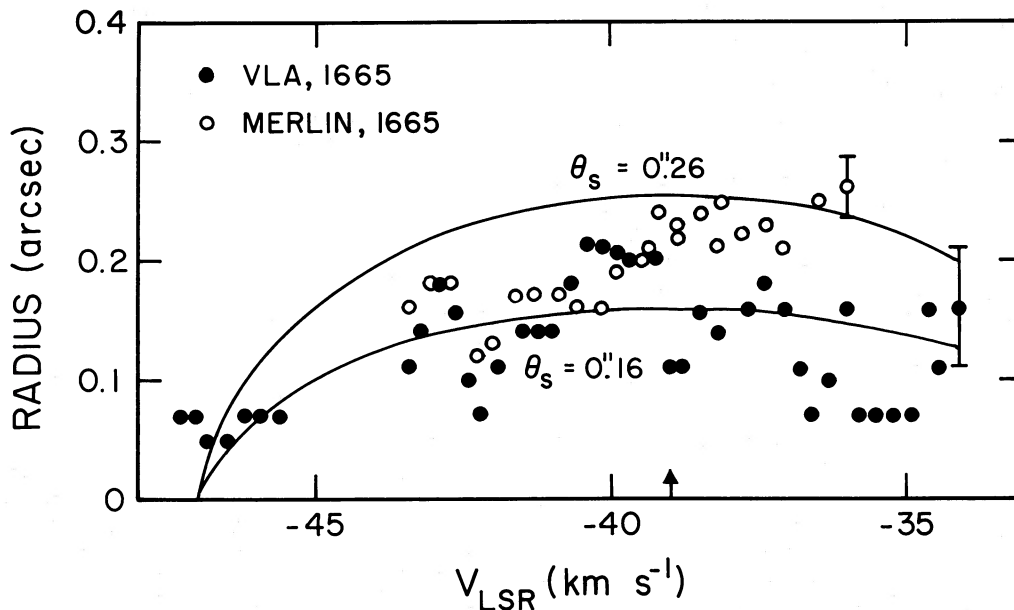


FIG. 5.—Angular radius of the 1665 MHz emission components from our adopted stellar position as a function of the radial velocity. VLA data (filled circles) are shown in Fig. 2; MERLIN data (empty circles) are shown in Fig. 3. Respective error bars are indicated, and the arrow indicates the adopted stellar velocity. The curves are computed from eq. (1) and represent the inner and outer radii of the maser region. Only VLA data points at $V < -45 \text{ km s}^{-1}$ and MERLIN data points have been considered for fitting the curves (§ IVd).

becomes much larger and the shape becomes more random. We consider this to be evidence that our adopted stellar position is reasonably well determined.

Figure 5 shows that there is good agreement of both the VLA and MERLIN data sets at $V < V_0$, but that the values of the radius determined by the VLA are systematically smaller at $V > V_0$. Because this result may be caused by spatial blending (see also § III), we consider only the VLA data points near $V = -47 \text{ km s}^{-1}$ and the MERLIN data points as significant.

The increase of radius as V increases from -47 km s^{-1} to higher velocities again confirms that radial expansion is the dominant kinematic component. However, the MERLIN data indicate that the maximum radius occurs between -39 and -36 km s^{-1} , suggesting a stellar radial velocity of at least -37.5 km s^{-1} , which is somewhat larger than our adopted value of -39 km s^{-1} (§ IVa). We cannot exclude this larger value entirely, but we prefer the adopted value because it is based on several independent indicators which are consistent with each other.

If the envelope is undergoing pure radial expansion, the angular radius-velocity relationship is given by

$$\theta = \theta_s \left[1 - \left(\frac{V - V_0}{V_e} \right)^2 \right]^{1/2}, \quad (1)$$

where θ is the angular radius at velocity V and θ_s is the actual shell radius in arcseconds. We have used this relationship with $V_0 = -39 \text{ km s}^{-1}$ and $V_e = 8 \text{ km s}^{-1}$ to plot the curves on Figure 5. The indicated radii are $0''.16$ and $0''.26$. We interpret these curves as representations of the inner and outer radii of the maser region. The mean shell radius $\langle \theta_s \rangle$ is thus $0''.21$ (54 AU at 250 pc), and the ratio of outer to inner radii is 1.6.

An empirical correlation between the radius and the mass-loss rate has been found by Bowers, Johnston, and Spencer (1981, 1983) and is supported on theoretical grounds by Huggins and Glassgold (1982), Deguchi (1982), Netzer and Knapp (1987), and Sun and Kwok (1987). The small radius suggests a mass-loss rate of $\sim 10^{-7 \pm 1} M_\odot \text{ yr}^{-1}$. This value is consistent with the infrared characteristics which indicate only a thin dust shell (e.g., Gehrz and Woolf 1971; Kruszewski and Coyne 1976) and with the low OH and H₂O maser luminosities which are comparable to those of other Mira variables with low mass-loss rates (Baud and Habing 1983; Bowers and Hagen 1984; Engels, Schmid-Burgk, and Walmsley 1986).

V. MODEL OF THE MASER REGION

Time-dependent behavior of the maser emission from U Ori has made it particularly difficult to determine the salient aspects of the data, let alone develop a model which adequately describes them. We submit that such a model should explain the following characteristics at 1665 MHz: a profile shape which has a peak of emission at $V \approx -47 \text{ km s}^{-1}$, stronger peaked features at about -42 and -36 km s^{-1} which correspond to the preflare peaks, and readily explicable emission near the stellar radial velocity of -39 km s^{-1} ; an angular distribution which has the east-west velocity discontinuity indicated by the line in Figure 3, the north-south velocity gradient in the eastern portion of the distribution, the incomplete ringlike structure at $V = -39 \text{ km s}^{-1}$, and the clustering of low-velocity emission near the center of the overall distribution. In addition, the model should be consistent with the profile structure and angular distribution observed at 1612 MHz and with the preflare OH, ($v = 0$) SiO, and H₂O data.

In this section we present a model which explains these aspects of the data, but we first consider several other possibilities which have been suggested in the literature.

a) Magnetic Field

Chapman and Cohen (1985) noted that a magnetic field could produce the broad, centrally peaked profile shape at 1665 MHz and a velocity gradient in the angular distribution. However, the clustering of -47 km s^{-1} emission near the center of the overall distribution in Figure 3 is inconsistent with this proposal. There also are not strong indications of Zeeman splitting, although there is evidence for linear or circular polarization in the OH profiles (Reid *et al.* 1979; Fix *et al.* 1980; Claussen and Fix 1982). Thus while the magnetic field may be important for determining the structure of the envelope, the observed distribution of maser features is more likely determined by the velocity field and the spatial distribution of the OH and the requisite pump radiation.

b) Acceleration

If the radial expansion velocity V_e varies smoothly with radius r from the star, then one can define a logarithmic velocity gradient ϵ such that

$$V_e = V_i (r/r_i)^\epsilon,$$

where V_i is the expansion velocity at the inner radius r_i of the maser shell. A large value of $\epsilon (> 1)$ also could produce a centrally peaked profile at 1665 MHz (Chapman and Cohen 1985). Such a model requires that the expansion velocity should increase from $\sim 3 \text{ km s}^{-1}$ (corresponding to the velocity ranges of the preflare OH, H₂O, and SiO in Fig. 4) to at least 8 km s^{-1} to account for the total velocity range of the OH. If this occurs in a shell with a ratio of outer to inner radii $r_o/r_i \approx 1.6$ (§ IVd), then $\epsilon \approx 2$.

We do not dismiss the possibility that some acceleration is present. Indeed, there is an increasing amount of evidence which supports values of $\epsilon \leq 0.5$ in the OH maser regions of circumstellar envelopes (Nguyen-Q-Rieu *et al.* 1979; Chapman and Cohen 1986; Bujarrabal *et al.* 1986). However, the acceleration model is not adequate to explain the velocity discontinuity in the angular distribution.

c) Rotation

This mechanism was suggested by Fix *et al.* (1980) as a possible explanation of the north-south velocity gradient in the eastern portion of the distribution in Figure 3. Clearly, rotation is not a primary component of the velocity field, since such a model would predict features at extreme low and high velocities to be distributed at the edge of the overall distribution and features at $V \approx V_0$ to be distributed near the center.

d) Geometry of the Emission Distribution

From the previous discussion, we find no compelling reason to adopt a velocity field which deviates significantly from constant radial expansion in the OH maser region. Nevertheless, we have computed simple, kinematic models for a wide range of combinations of rotation, acceleration, and shell thickness in order to understand their possible effects on the profile structure, angular distribution, and radius-velocity relationship. These calculations provided no satisfactory interpretation in the case where the emission is uniformly distributed throughout the shell. We therefore conclude that the complex nature of the data along with evidence for predominantly radial expansion require a complex geometric distribution of the emission.

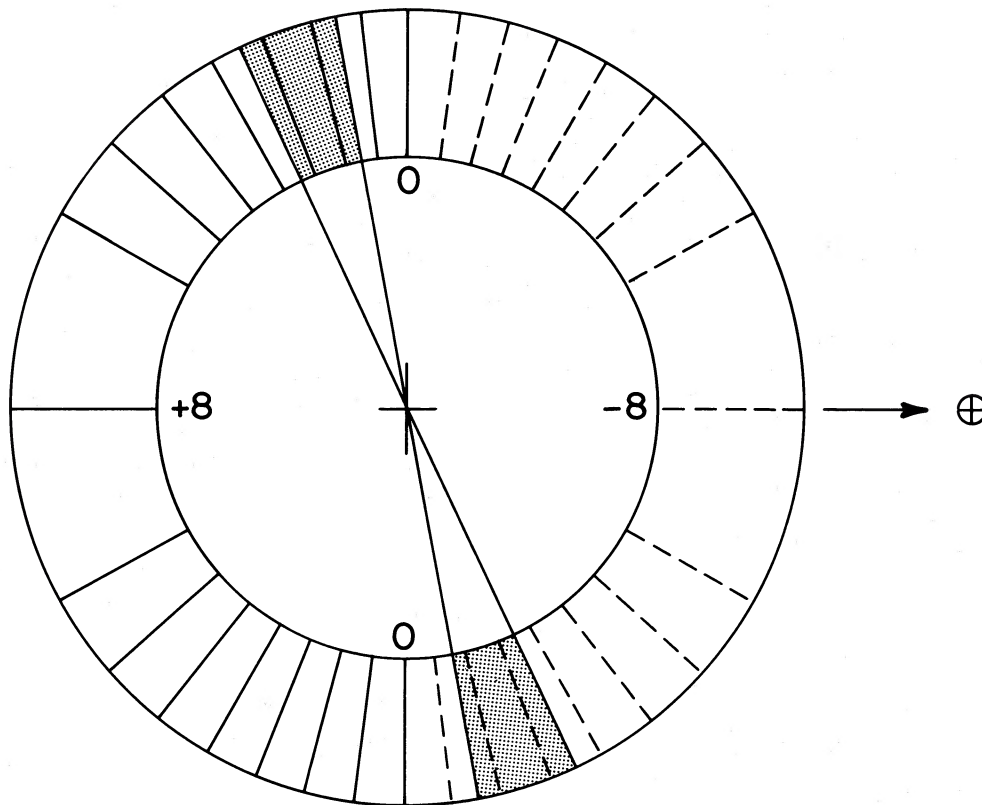


FIG. 6.—Model of the 1665 MHz emission distribution of U Ori in the plane perpendicular to the plane of the sky. Emission can arise anywhere inside an approximately spherical shell whose inner and outer radii are indicated by the annulus in the figure, but strongest emission occurs in the biconical density concentrations indicated by the shaded regions. The outflow velocity is 8 km s^{-1} in all directions. Dashed and solid lines connecting the boundaries of the annulus indicate the appropriate radial velocity along a given line of sight. The emission is linearly amplified along the line of sight to the Earth over the shell thickness or the velocity-coherent pathlength, whichever is smaller. A thermal velocity of 2 km s^{-1} is adopted for this model, and the ratio of the outer to inner radii is 1.6. The contrast ratio for the strength of saturated emission from the shaded and unshaded portions is 20:1.

We propose a model in which axisymmetric, biconical OH density concentrations are embedded in an approximately spherical gas distribution expanding at a constant radial velocity of 8 km s^{-1} . Maser emission can originate anywhere in the shell but the strongest emission preferentially emanates from the biconical lobes. A cross section of the shell in the plane perpendicular to the plane of the sky is shown in Figure 6, where the lines connecting the inner and outer radii of the annulus indicate the radial velocity of the gas as seen from the Earth. Maser emission originates from the annulus and is strongest in the shaded regions which denote the biconical lobes. The axis defined by the lobes is tilted to the line of sight by $\sim 70^\circ$ and is oriented approximately northeast by southwest in the plane of the sky. The diagonal line in Figure 3 thus represents the polar axis projected onto the plane of the sky.

The corresponding line profile is shown in Figure 7. The number of photons at velocity V and impact parameter p has been calculated from $N_{vp} = WL$, where W is a constant at a given V , which incorporates the effects of the spatial distribution of the inverted OH molecules, and where L is the velocity-coherent path length over which amplification can occur. L depends on the line-of-sight thickness of the annulus and on the Doppler broadening caused by thermal and microturbulent motions. We have adopted a value of 2 km s^{-1} for the Doppler broadening based on a kinetic temperature $\sim 1000 \text{ K}$ at a radius of 54 AU (see Goldreich and Scoville

1976). Our adopted value is only approximate since their model of the radial temperature dependence is derived for a cooler star (IRC + 10011) with a higher mass-loss rate, but we note that the Doppler broadening is only modestly dependent on the temperature ($\propto T^{1/2}$). The number of photons at velocity V for the edge-on annulus is then given by

$$N_v = \int_{p_1 = -r_0}^{p_2 = r_0} N_{vp} dp,$$

where the impact parameter p of an arbitrary point in the annulus is the distance between the star and the point projected onto the plane of the sky. The profile has been numerically computed, using a step size of $r_0/200$ for the impact parameter and for the line-of-sight path length. Our assumption that $N_{vp} \propto L$ is strictly true only for totally saturated emission. If the main-line emission is unsaturated (e.g., Jewell, Webber, and Snyder 1981), then $N_{vp} \propto e^L$ and the value of W is correspondingly smaller for a given output intensity.

Normally, the line profile for a shell expanding at constant velocity is doubly peaked at $V_0 \pm V_e$ because of the small velocity gradient along the line of sight to the star. These peaks are evident in Figure 7 but do not dominate the profile because of the stronger emission arising from the embedded biconical structure. To produce this profile we have assumed a saturated contrast ratio of 20:1 for the intensity of the shaded and unshaded regions and a shell thickness given by $r_o/r_i = 1.6$

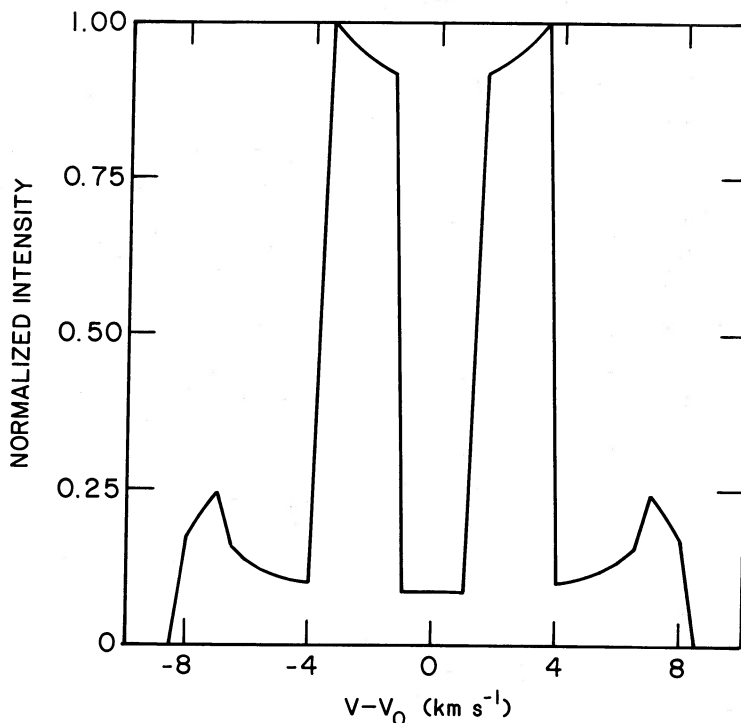


FIG. 7.—Normalized intensity as a function of radial velocity for the model shown in Fig. 6

(§ IVd). The model is relatively insensitive to the adopted shell thickness. The contrast ratio has been arbitrarily chosen to emphasize the emission arising from the biconical structure but also to illustrate the effects of weaker emission arising at high latitudes from the axis defined by the lobes. Clearly, the actual emission distribution is more complex, as is evident by the asymmetric velocity range relative to V_0 (e.g., Fig. 4) and by the difference between the shapes of the preflare and postflare emission profiles at 1665 MHz. Indeed, changes of the profile shape dictate that the contrast ratio changes with time. It is evident, however, that our model can account for the general features of the observed profile: i.e., weak emission at $(V - V_0 \approx -8 \text{ km s}^{-1})$, peaks at about $\pm 3 \text{ km s}^{-1}$ due to emission concentrated in the lobes, and significant emission near 0 km s^{-1} which can originate from gas at low or high latitudes relative to the lobes.

The model predicts that emission at velocities symmetric to the stellar radial velocity (i.e., $V_0 \pm \Delta V$) will appear as rings of identical radius centered about the star, but stronger emission from the biconical structure is more likely to be detected and will appear as arcs at opposite ends of the angular distribution with a separation which increases as V approaches V_0 . This model therefore explains the incomplete ring structure at $V \approx V_0$, the east-west velocity discontinuity which is apparent in Figure 3, and the clustering of low-velocity emission at $V \approx -47 \text{ km s}^{-1}$ near the center of the overall distribution. The north-south velocity gradient in the eastern portion of the shell is produced by azimuthal structure in the eastern lobe. In summary, this model provides a qualitatively consistent explanation of the profile structure and the angular distribution at 1665 MHz. The model indicates that the doubly peaked emission at 1612 MHz arises from the eastern lobe and from the near side of the shell along the line of sight to the star, consistent with its distribution in Figure 3.

The spatial distribution of the H_2O masers is less certain. The similarity of the velocity ranges of the H_2O masers and the preflare OH masers argues for similar spatial distributions. However, VLBI observations by Lada *et al.* (1981) show the H_2O masers to have a complex velocity structure and to be aligned along a position angle of -30° , identical to that of the line in Figure 3. Interpretation of H_2O data is difficult because the observed size and shape of the distribution can change with time (Johnston, Spencer, and Bowers 1985), but the VLBI result may suggest that the H_2O is distributed at high latitudes. We note that H_2O and main-line OH masers are distributed orthogonally in the plane of the sky for VX Sgr (Chapman and Cohen 1986).

It is likely that the ($v = 0$) SiO emission is distributed throughout the shell but concentrated in the biconical structures (like the OH) or else orthogonally to them (like the H_2O). If this emission were due to maser action (Nyman and Olofsson 1985), we would expect it to be close to the star in the chaotic velocity field of the ($v = 1$) SiO masers. In this case its velocity range should be much larger than observed (see Fig. 4). It appears, therefore, that the ($v = 0$) SiO emission is probably thermal, and its narrow, triangular profile shape is a consequence of the spatial variation of optical depth effects in the shell.

In summary, we submit that this model can account for the salient characteristics of the available data, as listed at the beginning of this section, and involves a minimum number of assumptions about the velocity field, spatial distribution, and detailed physical conditions of gas in the envelope. We do not exclude the possibility of a small amount of acceleration ($\epsilon \lesssim 0.5$) or rotation ($\lesssim 3 \text{ km s}^{-1}$ along the line of sight), but our calculations show that changes in the profile structure and angular distribution produced by velocity components of this magnitude are too small to be demonstrated convincingly from

the available data. The possible presence of such components introduces an uncertainty of about $\pm 1 \text{ km s}^{-1}$ to our adopted expansion velocity.

VI. IMPLICATIONS

a) *The Pump Mechanism*

It is generally thought that far-infrared ($\lambda \geq 35 \mu\text{m}$) pumping schemes can explain maser emission in the envelopes of evolved stars (Elitzur, Goldreich, and Scoville 1976; Elitzur 1978; Bujarrabal *et al.* 1980*a, b*; Morris and Bowers 1980), but near-infrared ($\lambda = 2.8 \mu\text{m}$) pumping may be possible in certain circumstances (Litvak and Dickinson 1972; Elitzur, Goldreich and Scoville 1976; Cimerman and Scoville 1980). Most of these models predict that main-line (1665/1667 MHz) emission should occur relatively close to the star ($< 10^{16} \text{ cm}$), at smaller radii than the 1612 MHz emission.

Interferometric data show that the actual situation is much more complicated, probably because of the wide range of physical conditions over which circumstellar masers can occur. At one extreme is U Ori with a maser shell radius of $\sim 10^{15} \text{ cm}$ and a mass-loss rate estimated to be $\sim 10^{-7} M_{\odot} \text{ yr}^{-1}$. In this case the masers at 1612 and 1665 MHz are distributed over similar regions. At the other extreme are stars like IRC +10420 (Bowers 1984) and OH 231.8+4.2 (Morris, Bowers, and Turner 1982; Bowers and Morris 1984) whose maser shell radii approach 10^{17} cm and whose mass-loss rates are $\sim 10^{-4} M_{\odot} \text{ yr}^{-1}$. Some of the 1667 MHz masers in IRC +10420 occur at a substantially larger radius than those at 1612 MHz, and this also appears to be the case for OH 231.8+4.2 (Morris and Bowers, unpublished).

No pumping model comprehensively addresses the wide range of physical conditions implicit for these cases, but the far-infrared, line-overlap model of Bujarrabal *et al.* (1980*b*) is promising since it appears to be extremely efficient over a large range of dust temperatures. For the highest dust temperature considered by them (450 K), the maximum gains at 1612 and 1665 MHz occur at comparable column densities, consistent with the comparable sizes of these maser regions in the case of U Ori.

Prior to the maser flare of 1974, this star was not considered to be particularly unusual. Garrigue and Mennessier (1980) subsequently showed that the light curve was shifted by 2 mag above the mean value in the year preceding the OH flare, and Wallerstein (1985) confirmed the unprecedented nature of this visual maximum. Garrigue and Mennessier proposed that a perturbation in the photosphere disturbed the light curve and then propagated outward to the inner dust shell ($r \approx 10 \text{ AU}$), where it altered the infrared radiation field which supplies pump radiation for the maser emission.

This idea is attractive in view of the short time scales over which the emission profiles changed dramatically and in view of the complex geometric distribution suggested in § V. For such a geometry we would expect the environment of gas in the biconical lobes to be considerably different than that of gas at high latitudes, promoting significantly different responses to the changes in the radiation field. With detailed modeling it therefore might be possible to examine the suggestion by Jewell, Webber, and Snyder (1981) that the 1612 and 1665 MHz masers have similar pump mechanisms which are critically dependent on a common parameter, but in opposite ways.

b) *The Mass-Loss Mechanism*

A question of great interest is whether or not the geometry proposed for U Orionis is typical for evolved stars. Biconical

(or bipolar) geometries have been found for a variety of related post-main-sequence objects, including carbon-rich giants (see Cohen 1985), oxygen-rich supergiants (see Bowers 1985; Chapman and Cohen 1986), and planetary nebulae (Balick 1987), but no compelling evidence for a substantially non-spherical outflow has yet been found for any oxygen-rich red giant other than the well-known bipolar nebula OH 231.8+4.2. However, this object is a binary star (Cohen *et al.* 1985), whereas, to our knowledge, U Ori is not.

Interferometric observations of OH masers associated with red giants demonstrate that in well-resolved cases the gas is expanding at an essentially constant velocity and is distributed in all directions relative to the star with an approximately spherical (or moderately elliptical) morphology (Bowers, Johnston, and Spencer 1983; Herman *et al.* 1985). The interpretive link between the observed maser structure and the underlying envelope structure is difficult to establish uniquely (e.g., Bowers 1985), but infrared speckle interferometry also shows little evidence of strongly asymmetric spatial distributions for the oxygen-rich red giants (Dyck *et al.* 1984; Cobb and Fix 1987). However, U Ori differs in an important way from other red giants whose OH emission has been mapped, because its shell radius is about an order of magnitude smaller. Thus we are probing a region of the envelope normally reserved for H_2O masers which, regrettably, are much more difficult to interpret.

Bowers (1985) has argued that the mass loss in oxygen-rich nonbinary red giants is not strongly directionally dependent over a time scale of 10^3 yr , but with U Ori we are sensitive to a much shorter time scale ($\sim 30 \text{ yr} = 54 \text{ AU}/8 \text{ km s}^{-1}$). It therefore is possible that we are witnessing a short-lived configuration. For example, gas may be channeled along a magnetic axis which is not aligned with the rotation axis of the star, or gas may be ejected biconically but in different directions at different times. Alternatively, this geometry may be long-lived, but the contrast between the physical conditions at low and high latitudes is, in many cases, insufficient to produce significant asymmetries in the OH or infrared distributions at larger distances from the star. We are currently mapping the maser emission from similar stars to explore these possibilities.

VII. CONCLUSION

The complex character of the microwave emission associated with U Orionis has heretofore made it difficult to determine even basic properties of the envelope. From consideration of all available OH, H_2O , and SiO data, we find that a model of axisymmetric, biconical OH density concentrations embedded in a spherical outflow at a constant velocity provides a qualitative basis for understanding the overall properties of the profile structures and the angular distributions. Such a geometry is known for other types of evolved objects, but this is the first indication that it may be applicable to oxygen-rich, nonbinary red giants. Detailed modeling of the envelope structure now seems possible and may lead to further insights into the nature of the flaring event. The unique, time-dependent behavior of the OH masers associated with U Orionis combined with the extremely small maser shell may have provided a fortuitous laboratory for the investigation of the OH maser pump mechanism and the mass loss mechanism.

We thank the National Radio Astronomy Observatory for providing observing time for this project and J. Herman for a careful reading of the manuscript.

REFERENCES

- Balick, B. 1987, *A.J.*, **94**, 671.
 Baud, B., and Habing, H. J. 1983, *Astr. Ap.*, **127**, 73.
 Bowers, P. F. 1984, *Ap. J.*, **279**, 350.
 ———. 1985, *Mass Loss from Red Giants*, ed. M. Morris and B. Zuckerman (*Ap. Space Sci. Lib.*, **117**, 189).
 Bowers, P. F., and Hagen, W. 1984, *Ap. J.*, **285**, 637.
 Bowers, P. F., Johnston, K. J., and Spencer, J. H. 1981, *Nature*, **291**, 382.
 ———. 1983, *Ap. J.*, **274**, 733.
 Bowers, P. F., and Morris, M. 1984, *Ap. J.*, **276**, 646.
 Bujarrabal, V., Destombes, J. L., Guibert, J., Marlière-Demuyne, C., Nguyen-Q-Rieu, and Omont, A. 1980a, *Astr. Ap.*, **81**, 1.
 Bujarrabal, V., Guibert, J., Nguyen-Q-Rieu, and Omont, A. 1980b, *Astr. Ap.*, **84**, 311.
 Bujarrabal, V., Planesas, P., Gómez-González, J., Martín-Pintado, J., and del Romero, A. 1986, *Astr. Ap.*, **162**, 157.
 Chapman, J. M., and Cohen, R. J. 1985, *M.N.R.A.S.*, **212**, 375.
 ———. 1986, *M.N.R.A.S.*, **220**, 513.
 Cimerman, M. 1979, *Ap. J. (Letters)*, **228**, L79.
 Cimerman, M., and Scoville, N. 1980, *Ap. J.*, **239**, 526.
 Claussen, M. J., and Fix, J. D. 1982, *Ap. J.*, **263**, 153.
 Cobb, M. L., and Fix, J. D. 1987, *Ap. J.*, **315**, 325.
 Cohen, M. 1985, *Mass Loss from Red Giants*, ed. M. Morris and B. Zuckerman (*Ap. Space Sci. Lib.*, **117**, 291).
 Cohen, M., Dopita, M. A., Schwartz, R. D., and Tielens, A. G. G. M. 1985, *Ap. J.*, **297**, 702.
 Deguchi, S. 1982, *Ap. J.*, **259**, 634.
 Diamond, P. J., Norris, R. P., Rowland, P. R., Booth, R. S., and Nyman, L. Å. 1985, *M.N.R.A.S.*, **212**, 1.
 Dyck, H. M., Zuckerman, B., Leinert, Ch., and Beckwith, S. 1984, *Ap. J.*, **287**, 801.
 Elitzur, M. 1978, *Astr. Ap.*, **62**, 305.
 Elitzur, M., Goldreich, P., and Scoville, N. 1976, *Ap. J.*, **205**, 384.
 Engels, D., Schmid-Burgk, J., and Walmsley, C. M. 1986, *Astr. Ap.*, **167**, 129.
 Fillit, R., Proust, D., and Lépine, J. R. D. 1977, *Astr. Ap.*, **58**, 281.
 Fix, J. D. 1979, *Ap. J. (Letters)*, **232**, L39.
 Fix, J. D., Mutel, R. L., Benson, J. M., and Claussen, M. L. 1980, *Ap. J. (Letters)*, **241**, L59.
 Garrigue, J. P., and Mennessier, M. O. 1980, *Astr. Ap.*, **81**, L13.
 Gehrz, R. D., and Woolf, N. J. 1971, *Ap. J.*, **165**, 285.
 Goldreich, P., and Scoville, N. 1976, *Ap. J.*, **205**, 144.
 Harvey, P. M., Bechis, K. P., Wilson, W. J., and Ball, J. A. 1974, *Ap. J. Suppl.*, **27**, 331.
 Herman, J., Baud, B., Habing, H. J., and Winnberg, A. 1985, *Astr. Ap.*, **143**, 122.
 Herman, J., and Habing, H. J. 1985, *Astr. Ap. Suppl.*, **59**, 523.
 Högbom, J. A. 1974, *Astr. Ap. Suppl.*, **15**, 417.
 Huggins, P. J., and Glassgold, A. E. 1982, *A.J.*, **87**, 1828.
 Jewell, P. R., Elitzur, M., Webber, J. C., and Snyder, L. E. 1979, *Ap. J. Suppl.*, **41**, 191.
 Jewell, P. R., Webber, J. C., and Snyder, L. E. 1981, *Ap. J.*, **249**, 118.
 Johnston, K. J., Spencer, J. H., and Bowers, P. F. 1985, *Ap. J.*, **290**, 660.
 Kruszewski, A., and Coyne, G. V. 1976, *A.J.*, **81**, 641.
 Kwok, S. 1976, *J.R.A.S. Canada*, **70**, 49.
 Lada, C. J., Blitz, L., Reid, M. J., and Moran, J. M. 1981, *Ap. J.*, **243**, 769.
 Lane, A. P. 1982, Ph.D thesis, University of Massachusetts.
 Lane, A. P., Johnston, K. J., Bowers, P. F., Spencer, J. H., and Diamond, P. J. 1987, *Ap. J.*, **323**, 756.
 Litvak, M. M., and Dickinson, D. F. 1972, *Ap. J. (Letters)*, **12**, 113.
 Morris, M., and Bowers, P. F. 1980, *A.J.*, **85**, 724.
 Morris, M., Bowers, P. F., and Turner, B. E. 1982, *Ap. J.*, **259**, 625.
 Morris, M., Redman, R., Reid, M. J., and Dickinson, D. F. 1979, *Ap. J.*, **229**, 257.
 Netzer, N., and Knapp, G. R. 1987, *Ap. J.*, **323**, 734.
 Nguyen-Q-Rieu, Laury-Micoulaut, C., Winnberg, A., and Schultz, G. V. 1979, *Astr. Ap.*, **75**, 351.
 Nyman, L.-Å., and Olofsson, H. 1985, *Astr. Ap.*, **147**, 309.
 ———. 1986, *Astr. Ap.*, **158**, 67.
 Pataki, L., and Kolena, J. 1974, *Bull. AAS*, **6**, 340.
 Reid, M. J., and Dickinson, D. F. 1976, *Ap. J.*, **209**, 505.
 Reid, M. J., Moran, J. M., Leach, R. W., Ball, J. A., Johnston, K. J., Spencer, J. H., and Swenson, G. W. 1979, *Ap. J. (Letters)*, **227**, L89.
 Reid, M. J., Muhleman, D. O., Moran, J. M., Johnston, K. J., and Schwartz, P. R. 1977, *Ap. J.*, **214**, 60.
 Snyder, L. E., Jewell, P. R., Dinger, A. S., Dickinson, D. F., and Buhl, D. 1986, *A.J.*, **92**, 416.
 Sun, J., and Kwok, S. 1987, *Astr. Ap.*, **185**, 258.
 Wallerstein, G. 1985, *Pub. A.S.P.*, **97**, 1001.
 Wilson, W. J., Schwartz, P. R., Neugebauer, G., Harvey, P. M., and Becklin, E. E. 1972, *Ap. J.*, **177**, 523.

P. F. BOWERS and K. J. JOHNSTON: Code 4130, Naval Research Laboratory, Washington, DC 20375-5000